Deformed-Skyrme-Hartree-Fock calculation of Hg isotopes

Yao-song Shen,[1,2,3] XiaoFeng Zhu,[4] and Zhongzhou Ren[5,6]
[1]*CCAST (World Laboratory), P.O. Box 8730, Beijing 100080, China*
[2]*Graduate School, China Academy of Engineering Physics, Beijing 100088, China*
[3]*Institute of Applied Physics and Computational Mathematics, Beijing 100088, China*
[4]*China Institute of Atomic Energy, P.O. Box 275, Beijing 102413, China*
[5]*Department of Physics, Nanjing University, Nanjing 210008, China*
[6]*Institute of Theoretical Physics, University of Tuebingen, D-72076 Tuebingen, Germany*
(Received 14 May 1998)

The ground-state properties of Hg isotopes are investigated by the deformed skyrme-Hartree-Fock (DSHF) model with new force parameters SKI4 [P. G. Reinhard and H. Flocard, Nucl. Phys. **A584**, 467 (1995)]. Calculations show that the deformed Skyrme-Hartree-Fock model with the above force parameters provides a good description of the binding energies, radii, and deformation parameters of Hg isotopes. Six kinds of configurations, which include a spherical shape, prolate one, oblate one, and three sets of triaxial shapes, are considered in our calculations, and this almost exhausts all possibilities of deformations for nuclei. A detailed discussion of the numerical results is given in this paper. [S0556-2813(99)02301-8]

PACS number(s): 21.10.Dr, 21.30.Fe, 21.60.Jz

I. INTRODUCTION

As a result of the experimental development of radioactive beams, a new field in nuclear physics has appeared recently: studies on exotic nuclei far from stability. The quality and quantity of experimental data on exotic nuclei have increased greatly in the past few years [1–4]. This provides a good opportunity to test and develop various nuclear structure models which have been proposed based on studies of nuclei near the stable line. It also gives us a chance to see the merits and drawbacks of various mean-field models when we apply them to all nuclei in the periodic table.

Among many open problems in this new field, the variation of nuclear shapes with neutron excess for an isotope chain has attracted both theoretical and experimental attention because it is directly related to the coupling between deformation degrees of freedom and isospin degrees of freedom. The chain of Hg isotopes is a good example to investigate the variation of shapes with neutron excesses because there are rich data on this isotope chain [5–16]. Previous studies [5–16] show that there are shape coexistences in many Hg isotopes and therefore their structures are more complicated than other nuclei. This will bring about a stringent restriction on the validity of various force parameters in mean-field models. Bengtsson *et al.* [5] have used the Woods-Saxon potential and the modified harmonic oscillator (Nillson) potential to calculate the properties of $^{182-188}$Hg in the triaxial gamma plane. They found that an oblate ground state appears for $^{178-188}$Hg [5]. Otten [3] has predicted that there may be triaxial shape in Hg isotopes. Patra *et al.* [6] and Yoshida and co-workers [7,8] have calculated the properties of Hg isotopes using a deformed relativistic mean-field (RMF) model with parameter set NL1. They conclude [6–8] that there are shape transitions from oblate ellipsoid to prolate ellipsoid at ^{178}Hg and from prolate ellipsoid to oblate ellipsoid at ^{188}Hg. A superdeformed ground state in ^{180}Hg is also reported in their papers [6–8]. However, Heyde *et al.* [9] have pointed out that some of the numerical results contradict experimental data for Hg isotopes. Therefore it is interesting to investigate the ground-state properties of Hg isotopes in detail.

The Skyrme-Hartree-Fock (SHF) model has proved to be a successful tool for a microscopical description of the ground-state properties of nuclei. Bonche *et al.* [10–12] have adumbrated shape isomerism and concomitant superdeformation in the Hg isotopes using the SHF model with parameter set SKM*. They also studied the depopulation of the superdeformation by the generator coordinate method [10–12]. But it is pointed out recently that the traditional force parameters in the Skyrme parametrization (such as SKM*) is determined by fitting the ground-state properties of several nuclei near the stable line and therefore they fail to reproduce the observed isotope shifts in Sr and Pb elements [17,18]. In order to solve the above problem in the SHF model, Reihard and Flocard [18] have introduced isospin degrees of freedom in the spin-orbit term, i.e., to replace the normal spin-orbit potential with a generalized spin-orbit potential. A new set of the force parameters SKI4 has been proposed by a fit of the ground-state properties of nuclei near the stable line and far from the stable line [18].

Recently, we have used the new parameter set SKI4 to calculate the ground state properties of spherical nuclei such as Ni, Sn, and Pb isotopes [19,20]. It is found that the SKI4 has succeeded in describing the above nuclei both near the stable line and far from the stable line [19,20]. The successes of the force SKI4 for spherical nuclei encourage us to apply this force to deformed nuclei. In this article, we will report theoretical results of Hg isotopes using the parameter set SKI4 where possible configurations of deformations such as triaxial deformations will be included. In our calculation, the single-particle wave functions are expressed in a three-dimensional Cartesian-mesh representation. One of the advantages of the mesh representation is that we can treat the various shapes such as triaxial deformation and superdeformation without preparing a specific basis for each shape [13,14]. We have calculated the ground-state properties of

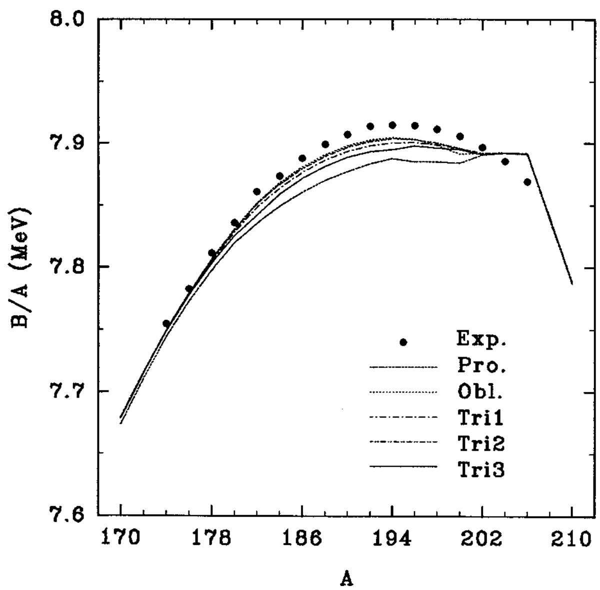

FIG. 1. The binding energy per nucleon of Hg isotopes for five cases.

light C isotopes and found that they agree well with experiment data [21]. Here we will report a large-scale calculation on heavy Hg isotopes.

This paper is organized in the following way. Section II is a short description of the framework of the model and method. In Sec. III, we give the numerical results and a discussion. Section IV is a summary.

II. MODEL AND METHOD

As the Skyrme-Hartree-Fock model is a standard theory and all the formulations can be found in Refs. [19, 20], here we only give a short description on the framework of the SHF model with new force parameters SKI4 [18].

The SHF equation is written as follows:

$$\left[-\nabla\cdot\frac{\hbar^2}{2m_q^*(\mathbf{r})}\nabla+U_q(\mathbf{r})+W_q(\mathbf{r})(-i)(\nabla\times\sigma)\right]\phi_i=e\phi_i, \tag{1}$$

where $(\hbar^2/2m_q^*)(\mathbf{r})$ is the inverse mass, $U_q(\mathbf{r})$ is the potential, and $W_q(\mathbf{r})$ is the spin-orbit potential. A detailed description of the above terms can be found in Refs. [19, 20]. For the normal Skyrme force, the neutron density dependence is linear for the inverse mass and spin-orbit potentials [18]:

$$\frac{\hbar^2}{2m_q^*(\mathbf{r})}=\frac{\hbar^2}{2m}+b_1\rho(\mathbf{r})+b_1'\rho_q(\mathbf{r}), \tag{2}$$

$$W_q(\mathbf{r})=b_4[\nabla\rho(\mathbf{r})+\nabla\rho_q(\mathbf{r})]. \tag{3}$$

Reinhard and Flocard [18] have introduced an additional coefficient b_4' in the spin-orbit term in a generalized Skyrme functional:

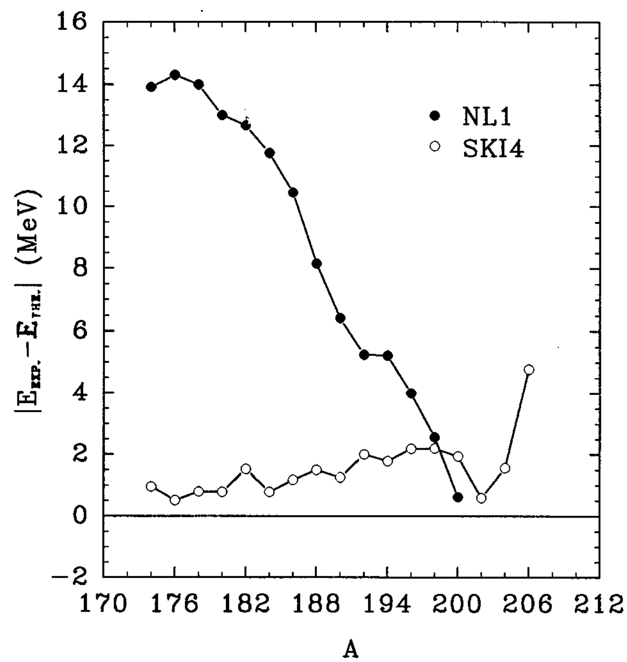

FIG. 2. The absolute difference of the binding energy between theoretical results and experimental data for Hg isotopes.

$$\varepsilon_{ls}=-\int d^3r\left\{b_4\rho\nabla J+\sum_{q\in\{p,n\}}b_4'\rho_q\nabla J_q\right\}, \tag{4}$$

where J is the spin density and its definition can be found in Refs. [19, 20]. The spin-orbit potential W for the nucleus becomes [18]

$$W_q(\mathbf{r})=b_4\nabla\rho(\mathbf{r})+b_4'\nabla\rho_q(\mathbf{r}). \tag{5}$$

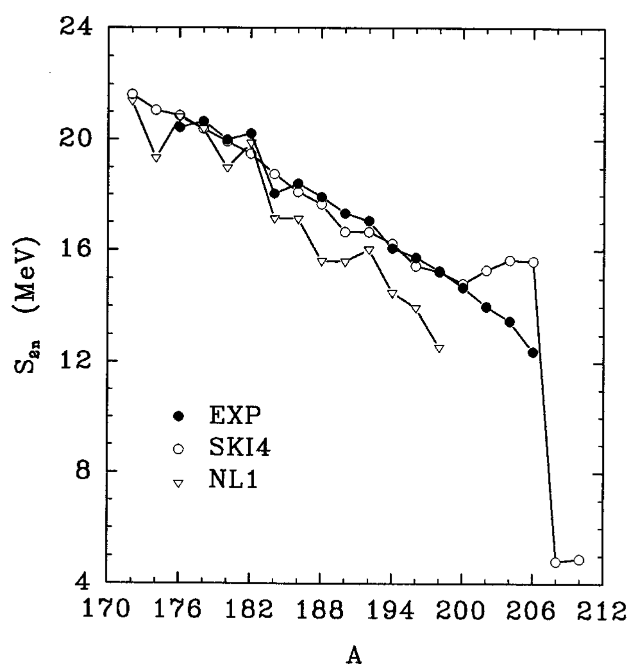

FIG. 3. Two-neutron separation energy of Hg isotopes. The open circles are calculated values with SKI4. Experimental data are denoted by the solid circles.

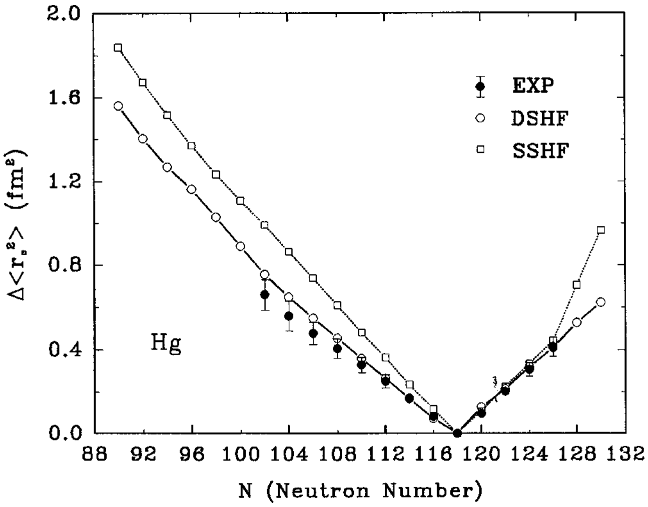

FIG. 4. The isotope shifts of Hg nuclei in DSHF and SSHF with SKI4. The experimental isotope shifts for Hg isotopes [24] are also shown for comparison.

The values of SKI4 are [18] $t_0=-1855.83$, $t_1=473.829$, $t_2=1006.86$, $t_3=9703.61$, $x_0=0.4051$, $x_1=-2.8891$, $x_2=-1.3252$, $x_3=1.1452$, $b_4=183.097$, $b_4'=-180.351$, and $\alpha=0.25$.

The quadrupole moments are defined as [15]

$$Q_x^{n,p}=\langle 2x^2-y^2-z^2\rangle^{n,p}, \tag{6}$$

$$Q_y^{n,p}=\langle 2y^2-z^2-x^2\rangle^{n,p}, \tag{7}$$

$$Q_z^{n,p}=\langle 2z^2-x^2-y^2\rangle^{n,p}, \tag{8}$$

$$Q_0^{n,p}=\sqrt{\frac{2(Q_x^2+Q_y^2+Q_z^2)^{n,p}}{3}}, \tag{9}$$

$$Q_{20}^{n,p}=\sqrt{\frac{5}{4\pi}}\langle 2z^2-x^2-y^2\rangle^{n,p}=\sqrt{\frac{5}{4\pi}}\,Q_z^{n,p}, \tag{10}$$

$$Q_{22}^{n,p}=\sqrt{\frac{15}{8\pi}}\langle x^2-y^2\rangle^{n,p}=\sqrt{\frac{5}{24\pi}}(Q_x^{n,p}-Q_y^{n,p}), \tag{11}$$

and the hexadecapole moments are calculated by [15]

$$Q_{40}^{n,p}=\sqrt{\frac{9}{64\pi}}\langle 3(x^2+y^2)^2-24z^2(x^2+y^2)+8z^4\rangle^{n,p}, \tag{12}$$

$$Q_{42}^{n,p}=\sqrt{\frac{45}{32\pi}}\langle 3y^4-x^4-6z^4-6x^2z^2\rangle^{n,p}, \tag{13}$$

$$Q_{44}^{n,p}=\sqrt{\frac{315}{128\pi}}\langle x^4-6x^2y^2+y^4\rangle^{n,p}. \tag{14}$$

The quadrupole deformation parameters β_2 and γ_2 and the hexadecupole deformation parameters β_4, γ_4, and δ_4 are given by the expressions

$$\beta_2^{n,p}=\sqrt{a_{20n,p}^2+2a_{22n,p}^2}, \tag{15}$$

$$\gamma_2^{n,p}=\arctan\left[\sqrt{2}\,\frac{a_{22n,p}}{a_{20n,p}}\right], \tag{16}$$

$$\beta_4^{n,p}=\sqrt{a_{4n,p}^2+b_{4n,p}^2+c_{4n,p}^2}, \tag{17}$$

$$\gamma_4^{n,p}=\arctan\left[\frac{c_{4n,p}}{b_{4n,p}}\right], \tag{18}$$

$$\delta_4^{n,p}=\arcsin\left[\sqrt{\frac{b_{4n,p}^2+c_{4n,p}^2}{a_{4n,p}^2+b_{4n,p}^2+c_{4n,p}^2}}\right], \tag{19}$$

where

$$a_{4n,p}=\sqrt{\frac{7}{12}}\,a_{40n,p}+\sqrt{\frac{5}{6}}\,a_{44n,p}, \tag{20}$$

$$b_{4n,p}=\sqrt{\frac{5}{12}}\,a_{40n,p}-\sqrt{\frac{7}{6}}\,a_{44n,p}, \tag{21}$$

$$c_{4n,p}=-\sqrt{2}a_{42n,p}. \tag{22}$$

The coefficients a_{20}, a_{22}, a_{40}, a_{42}, and a_{44} are solutions of the coupled equations [15]

$$Q_{20}^{n,p}=2C_{n,p}R_0^2\left[a_{20n,p}+\frac{2}{7}\sqrt{\frac{5}{\pi}}(a_{20n,p}^2-a_{22n,p}^2)\right], \tag{23}$$

$$Q_{22}^{n,p}=2C_{n,p}R_0^2\left[a_{22n,p}-\frac{4}{7}\sqrt{\frac{5}{\pi}}\,a_{20n,p}a_{22n,p}\right], \tag{24}$$

$$Q_{40}^{n,p}=2C_{n,p}R_0^4\left[a_{40n,p}+\frac{3}{7}\sqrt{\frac{1}{\pi}}(3a_{20n,p}^2+a_{22n,p}^2)\right], \tag{25}$$

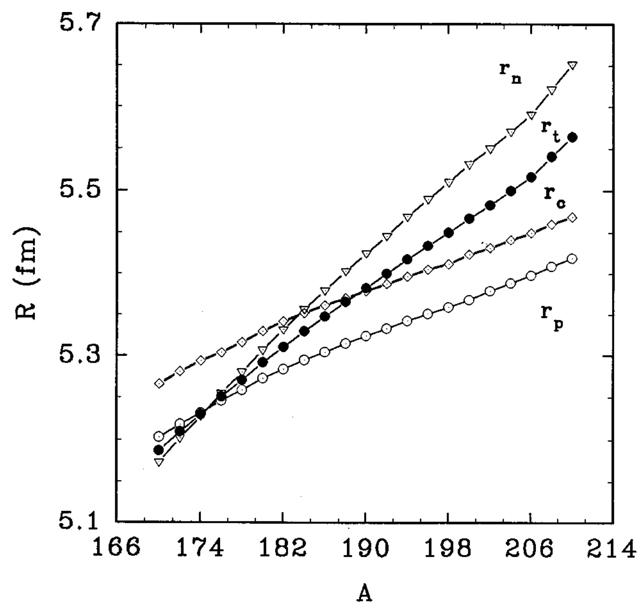

FIG. 5. The variation of nuclear radii with nucleon numbers. (r_n is the rms radius of neutron density distributions, r_p is the rms radius of proton density distributions, r_t is the rms radius of matter density distributions, and r_c is the rms radius of charge density distributions.)

TABLE I. Binding energies (MeV) and quadrupole deformation parameters β_2 and γ_2 (in degrees) obtained with the SK14. Experimental binding energies are taken from Ref. [23] and value labeled with # is the datum estimated from systematic trends. RMF-NL1 results [6] are listed for comparison.

		SK14					NL1		Expt.	
		E_B	β_2^p	γ_2^p	β_2^n	γ_2^n	E_B	β_p	E_B	$\|\beta_p\|$
^{170}Hg	sph	1304.40								
	pro	1304.61	0.07	0.00	0.08	0.00	1321.69	0.03		
	obl	1305.59	0.10	60.00	0.10	60.00	1322.48	−0.02		
	tri1	1305.41	0.10	43.03	0.10	37.96				
	tri2	1305.56	0.10	49.94	0.10	45.78				
	tri3	1305.37	0.09	35.11	0.09	28.17				
^{172}Hg	sph	1325.90								
	pro	1326.33	0.08	0.00	0.09	0.00	1343.57	0.05		
	obl	1327.24	0.10	60.00	0.11	60.00	1343.88	−0.07		
	tri1	1327.11	0.10	41.81	0.11	37.33				
	tri2	1327.19	0.10	49.20	0.10	46.78				
	tri3	1327.09	0.10	33.96	0.10	27.22				
^{174}Hg	sph	1347.10								
	pro	1347.51	0.09	0.00	0.10	0.00	1362.21	0.06		
	obl	1348.42	0.11	60.00	0.11	60.00	1363.23	−0.04		
	tri1	1348.38	0.10	41.99	0.11	37.26			1349.32#	
	tri2	1348.38	0.11	49.72	0.11	45.86				
	tri3	1348.32	0.10	33.51	0.11	27.24				
^{176}Hg	sph	1367.80								
	pro	1368.08	0.07	0.00	0.09	0.00	1382.82	0.28		
	obl	1369.20	0.11	60.00	0.12	60.00	1384.05	−0.08		
	tri1	1369.11	0.10	42.18	0.11	38.27				1369.76
	tri2	1369.16	0.11	49.13	0.12	46.51				
	tri3	1368.99	0.10	35.10	0.10	29.69				
^{178}Hg	sph	1388.10								
	pro	1388.00	0.07	0.00	0.07	0.00	1404.45	0.31		
	obl	1389.55	0.11	60.00	0.13	60.00	1402.79	−0.15		
	tri1	1389.36	0.10	44.34	0.11	41.64			1390.43	
	tri2	1389.54	0.11	49.86	0.12	48.10				
	tri3	1389.08	0.09	37.12	0.10	33.03				
^{180}Hg	sph	1407.60								
	pro	1407.55	0.06	0.00	0.07	0.00	1422.60	0.33		
	obl.	1409.53	0.12	60.00	0.14	60.00	1421.85	−0.33		
	tri1	1409.13	0.10	45.14	0.11	44.05			1410.44#	
	tri2	1409.45	0.12	50.80	0.13	50.78				
	tri3	1408.63	0.09	38.52	0.10	35.17				
^{182}Hg	sph	1427.20								
	pro	1426.05	0.06	0.00	0.07	0.00	1443.27	0.34		
	obl	1429.00	0.13	60.00	0.15	60.00	1443.33	−0.22		
	tri1	1428.36	0.11	45.81	0.12	44.81			1430.67	0.17
	tri2	1428.90	0.12	51.20	0.13	51.08				
	tri3	1427.30	0.10	36.40	0.11	32.57				
^{184}Hg	sph	1445.20								
	pro	1444.21	0.06	0.00	0.07	0.00	1460.47	0.33		
	obl	1447.75	0.13	60.00	0.16	60.00	1459.03	−0.23		
	tri1	1446.92	0.11	46.13	0.13	45.50			1448.71#	0.16
	tri2	1447.51	0.12	52.10	0.13	51.87				
	tri3	1446.08	0.10	37.80	0.11	35.34				
^{186}Hg	sph	1462.20								
	pro	1462.05	0.08	0.00	0.09	0.00	1477.59	0.29		
	obl	1465.83	0.13	60.00	0.15	60.00	1476.65	−0.21		
	tri1	1465.03	0.11	45.70	0.13	45.13			1467.13	0.24
	tri2	1465.60	0.12	51.16	0.13	50.78				
	tri3	1464.14	0.10	36.85	0.11	34.03				

TABLE I. (*Continued*).

		SK14					NL1		Expt.	
		E_B	β_2^p	γ_2^p	β_2^n	γ_2^n	E_B	β_p	E_B	$\lvert\beta_p\rvert$
	sph	1479.79								
	pro	1479.56	0.08	0.00	0.10	0.00	1492.90	0.28		
^{188}Hg	obl	1483.47	0.13	60.00	0.14	60.00	1493.20	−0.17		
	tri1	1482.65	0.11	43.79	0.13	43.60			1485.05$^{\#}$	0.14
	tri2	1483.22	0.12	51.00	0.14	50.38				
	tri3	1481.71	0.10	35.65	0.12	32.42				
	sph	1496.50								
	pro	1496.67	0.08	0.00	0.10	0.00	1508.20	0.27		
^{190}Hg	obl	1500.62	0.13	60.00	0.15	60.00	1508.79	−0.17		
	tri1	1499.76	0.12	44.00	0.14	43.36			1502.37$^{\#}$	0.15
	tri2	1500.42	0.12	50.36	0.14	50.77				
	tri3	1498.85	0.11	35.71	0.12	30.94				
	sph	1513.10								
	pro	1513.66	0.09	0.00	0.11	0.00	1522.99	0.25		
^{192}Hg	obl	1517.34	0.12	60.00	0.14	60.00	1524.69	−0.16		
	tri1	1516.46	0.11	44.17	0.13	43.88			1519.43$^{\#}$	0.14
	tri2	1517.11	0.12	50.64	0.14	50.43				
	tri3	1515.55	0.11	32.77	0.12	28.40				
	sph	1529.59								
	pro	1530.21	0.09	0.00	0.11	0.00	1538.21	0.12		
^{194}Hg	obl	1533.51	0.12	60.00	0.14	60.00	1540.71	−0.14		
	tri1	1532.67	0.11	43.14	0.13	44.20			1535.50	0.13
	tri2	1533.33	0.12	50.10	0.14	50.07				
	tri3	1531.66	0.10	31.45	0.12	25.80				
	sph	1545.27								
	pro	1545.50	0.08	0.00	0.09	0.00	1553.67	0.11		
^{196}Hg	obl	1549.06	0.12	60.00	0.14	60.00	1555.21	−0.14		
	tri1	1548.60	0.10	43.47	0.11	41.86			1551.23	0.12
	tri2	1549.02	0.11	49.72	0.12	48.78				
	tri3	1548.00	0.10	35.91	0.11	33.57				
	sph	1561.57								
	pro	1561.24	0.08	0.00	0.08	0.00	1567.81	0.08		
^{198}Hg	obl	1563.88	0.11	60.00	0.12	60.00	1569.17	−0.12		
	tri1	1564.07	0.10	43.73	0.11	40.62			1566.50	0.11
	tri2	1564.30	0.10	49.13	0.11	46.90				
	tri3	1563.52	0.09	36.54	0.10	34.19				
	sph	1576.60								
	pro	1576.86	0.07	0.00	0.07	0.00	1580.58	0.04		
^{200}Hg	obl	1578.27	0.10	60.00	0.11	60.00	1581.73	−0.10		
	tri1	1579.17	0.09	43.66	0.10	41.39			1581.20	0.10
	tri2	1579.26	0.09	49.72	0.10	47.17				
	tri3	1579.00	0.09	36.82	0.09	34.69				
	sph	1594.58								
	pro	1593.92	0.03	0.00	0.02	0.00				
	obl	1594.21	0.05	60.00	0.05	60.00				
^{202}Hg	tri1	1593.93	0.03	37.66	0.03	38.76			1595.18	
	tri2	1594.25	0.05	49.35	0.05	50.32				
	tri3	1594.00	0.03	24.07	0.03	27.19				

TABLE I. (*Continued*).

		SK14					NL1		Expt.	
		E_B	β_2^p	γ_2^p	β_2^n	γ_2^n	E_B	β_p	E_B	$\lvert\beta_p\rvert$
^{204}Hg	sph	1610.24							1608.67	
	pro	1609.96	0.01	0.00	0.01	0.00				
	obl	1610.06	0.01	60.00	0.01	60.00				
	tri1	1610.07	0.02	34.44	0.02	36.54				
	tri2	1610.05	0.02	43.52	0.02	44.61				
	tri3	1610.05	0.02	22.83	0.02	25.11				
^{206}Hg	sph	1625.85							1621.06	
	pro	1625.57	0.01	0.00	0.01	0.00				
	obl	1625.75	0.01	60.00	0.01	60.00				
	tri1	1625.70	0.01	32.88	0.01	32.10				
	tri2	1625.63	0.01	42.47	0.01	42.11				
	tri3	1625.62	0.01	21.72	0.01	21.26				
^{208}Hg	sph	1630.30								
	pro	1630.20	0.02	0.00	0.02	0.00				
	obl	1630.56	0.02	60.00	0.02	60.00				
	tri1	1630.52	0.02	45.07	0.03	44.51				
	tri2	1630.65	0.02	50.78	0.03	49.86				
	tri3	1630.50	0.02	30.51	0.03	33.68				
^{210}Hg	sph	1635.05								
	pro	1635.31	0.03	0.00	0.04	0.00				
	obl	1635.39	0.02	60.00	0.03	60.00				
	tri1	1635.40	0.02	36.67	0.03	36.71				
	tri2	1635.56	0.03	46.28	0.03	45.80				
	tri3	1635.45	0.03	19.83	0.04	19.62				

$$Q_{42}^{n,p}=2C_{n,p}R_0^4\left[a_{42n,p}+\frac{3}{7}\sqrt{\frac{15}{\pi}}\,a_{20n,p}a_{22n,p}\right], \quad (26)$$

$$Q_{44}^{n,p}=2C_{n,p}R_0^4\left[a_{44n,p}+3\sqrt{\frac{15}{14\pi}}\,a_{22n,p}^2\right], \quad (27)$$

with

$$C_p=\frac{3Z}{4\pi}, \quad C_n=\frac{3N}{4\pi}, \quad R_0=1.2A^{1/3}.$$

At the beginning of the calculations, the code needs the input of deformations which are controlled by IQ1 and IQ2. We use six kinds of configurations as our inputs (IQ1,IQ2): (0,0) is the spherical case (sph), (1,0) is the prolate case (pro), (0,1) is the oblate case (obl), (1,1) is the first triaxial case (tri1), (1,2) is the second triaxial case (tri2), and (2,1) is the third triaxial case (tri3). In the spherical case, $\beta_2=0$ and $\beta_4=0$; in the prolate case, $\gamma_2=0$, $\gamma_4=0$, and $\delta_4=\arccos(\sqrt{7/12})$; in the oblate case, $\gamma_2=\pi/3$, $\gamma_4=\pi/3$, and $\delta_4=\pi-\arccos(\sqrt{7/12})$; and in the triaxial case, $0<\gamma<\pi/3$.

Tajima *et al.* [14] have considered a correction for the error of the total binding energy due to the finite mesh size for the code in the three-dimensional Cartesian-mesh representation, but we use a very small mesh size $a=0.65$ fm in our calculation and thus the difference of the binding energy between the spherical SHF code and deformed SHF code is less than 0.1% for a spherical nucleus such as ^{208}Pb. This avoids inaccurately correcting the total energy as done in Ref. [14]. The only expense for this is to prolong the computation time (it takes 6 h of CPU time to get one solution for one Hg nucleus and the total CPU time in our calculation is about 800 h in the SGI workstation indigo11).

The neutron pairing correlations have been calculated with the force constant $G_n=g_n/(11+N)$ with $g_n=13.5$ MeV for neutrons and $G_p=g_p/(11+Z)$ with $g_p=16.5$ MeV for protons [13].

The mean field localizes the nucleus and thus breaks translational invariance which results in the center of mass of the whole nucleus oscillating in the mean field, but the spurious excitation of the center of mass has to be eliminated. A simple and reliable treatment of the center-of-mass correction is [22]

$$E_{\text{c.m.}}=\frac{\langle P_{\text{c.m.}}^2\rangle}{2Am},$$

$$\langle P_{\text{c.m.}}^2\rangle=\sum_\beta \omega_\beta\langle\phi_\beta|\hat{p}^2|\phi_\beta\rangle-\sum_{\alpha\beta}\left[\omega_\alpha\omega_\beta+\sqrt{\omega_\alpha(1-\omega_\alpha)\omega_\beta(1-\omega_\beta)}\right]|\langle\phi_\alpha|\hat{p}|\phi_\beta\rangle|^2, \quad (28)$$

where $P_{\text{c.m.}}=\Sigma_i\hat{p}_i$ is the total momentum operator.

TABLE II. The proton and neutron quadrupole moments Q_x, Q_y, and Q_z, and Q_0 obtained with the SK14.

		Proton (fm^2)				Neutron (fm^2)			
		Q_x	Q_y	Q_z	Q_0	Q_x	Q_y	Q_z	Q_0
	pro	−94.62	−94.62	189.24	189.24	−122.98	−122.98	245.96	245.96
	obl	124.25	−248.50	124.25	248.50	140.10	−280.20	140.10	124.25
^{170}Hg	tri1	48.84	−238.91	190.07	252.44	29.94	−268.21	238.27	293.95
	tri2	82.75	−256.77	174.02	262.13	78.02	−289.81	211.79	299.92
	tri3	13.11	−215.65	202.54	241.79	−19.32	−240.27	259.58	289.23
	pro	−108.12	−108.12	216.24	216.24	−145.83	−145.83	291.66	291.66
	obl	135.09	−270.18	135.09	270.18	158.86	−317.72	158.86	317.72
^{172}Hg	tri1	45.31	−250.00	204.69	266.40	24.55	−292.81	268.26	324.86
	tri2	82.81	−268.31	185.50	274.79	79.80	−315.42	235.62	328.00
	tri3	8.30	−224.87	216.57	255.00	−27.49	−261.39	288.88	318.88
	pro	−118.39	−118.39	236.78	236.78	−163.66	−163.66	327.32	327.32
	obl	139.56	−279.12	139.56	279.12	170.30	−340.60	170.30	340.60
^{174}Hg	tri1	46.28	−250.52	204.24	266.60	29.04	−303.95	274.91	335.47
	tri2	82.99	−272.65	189.66	279.52	82.79	−332.18	249.39	345.83
	tri3	6.19	−235.94	229.75	268.94	−30.53	−284.35	314.88	347.31
	pro	−103.85	−103.85	207.70	207.70	−143.39	−143.39	286.78	286.78
	obl	149.87	−299.74	149.87	299.74	189.40	−378.80	189.40	378.80
^{176}Hg	tri1	49.28	−264.38	215.10	281.18	37.22	−331.72	294.50	363.47
	tri2	86.85	−283.56	196.71	290.56	92.70	−357.71	265.01	371.28
	tri3	13.62	−229.60	215.98	257.62	−14.82	−283.55	298.37	336.30
	pro	−92.02	−92.02	184.04	184.04	−125.02	−125.02	250.04	250.04
	obl	156.16	−312.32	156.16	312.32	204.26	−408.52	204.26	408.52
^{178}Hg	tri1	58.21	−257.34	199.13	269.89	59.85	−331.95	272.10	353.85
	tri2	93.70	−294.78	201.08	301.23	109.75	−384.71	274.96	396.36
	tri3	22.29	−225.00	202.71	247.94	5.13	−283.78	278.65	324.77
	pro	−86.61	−86.61	173.22	173.22	−118.45	−118.45	236.90	236.90
	obl	166.51	−333.02	166.51	333.02	225.72	−451.44	225.72	451.44
^{180}Hg	tri1	65.02	−272.59	207.57	284.75	79.01	−364.48	285.47	383.48
	tri2	102.17	−306.79	204.62	312.44	131.56	−415.15	283.59	424.33
	tri3	27.08	−230.09	203.01	251.52	19.00	−298.60	279.60	334.37
	pro	−85.27	−85.27	170.54	170.54	−118.64	−118.64	237.28	237.28
	obl	171.59	−343.18	171.59	343.18	241.35	−482.70	241.35	482.70
^{182}Hg	tri1	69.26	−291.71	222.45	304.83	92.30	−406.32	314.02	426.01
	tri2	109.25	−322.21	212.96	327.72	151.03	−452.83	301.80	461.13
	tri3	20.28	−245.99	225.71	273.09	1.33	−333.43	332.10	384.24
	pro	−90.03	−90.03	180.06	180.06	−131.44	−131.44	262.88	262.88
	obl	175.44	−350.88	175.44	350.88	254.31	−508.62	254.31	508.62
^{184}Hg	tri1	72.94	−292.33	219.39	304.31	100.87	−421.66	320.79	440.36
	tri2	111.31	−313.43	202.12	317.79	158.34	−455.12	296.78	462.09
	tri3	27.07	−248.39	221.32	272.54	20.40	−348.54	328.14	391.21
	pro	−113.93	−113.93	227.86	227.86	−174.22	−174.22	348.44	348.44
	obl	174.38	−348.76	174.38	348.76	259.29	−518.58	259.29	518.58
^{186}Hg	tri1	72.70	−294.98	222.28	307.36	101.75	−438.43	336.68	458.93
	tri2	110.81	−327.95	217.14	333.64	160.71	−488.47	327.76	497.90
	tri3	23.11	−256.92	233.81	284.26	11.42	−372.81	361.39	424.04

TABLE II. (*Continued*).

		Proton (fm^2)				Neutron (fm^2)			
		Q_x	Q_y	Q_z	Q_0	Q_x	Q_y	Q_z	Q_0
	pro	−121.67	−121.67	243.34	243.34	−193.36	−193.36	386.72	386.72
	obl	176.05	−352.10	176.05	352.10	267.20	−534.40	267.20	534.40
^{188}Hg	tri1	67.35	−305.59	238.24	321.12	94.54	−465.77	371.23	492.40
	tri2	109.26	−328.51	219.25	334.59	160.60	−501.00	340.40	511.65
	tri3	17.38	−264.59	247.21	295.99	−1.53	−394.81	396.34	456.77
	pro	−120.12	−120.12	240.24	240.24	−197.44	−197.44	394.88	394.88
	obl	172.11	−344.22	172.11	344.22	267.40	−534.80	267.40	534.80
^{190}Hg	tri1	65.93	−306.36	240.43	322.50	94.90	−478.24	383.34	506.41
	tri2	108.33	−334.46	226.13	341.31	162.85	−520.36	357.51	532.36
	tri3	13.10	−265.00	251.90	298.72	−13.81	−403.17	416.98	473.72
	pro	−131.59	−131.59	263.18	263.18	−222.24	−222.24	444.48	444.48
	obl	165.73	−331.46	165.73	331.46	263.77	−527.54	263.77	527.54
^{192}Hg	tri1	67.01	−306.38	239.37	322.14	101.75	−488.77	387.02	515.77
	tri2	107.88	−327.32	219.44	333.60	167.73	−521.05	353.32	531.95
	tri3	2.52	−269.82	267.30	310.12	−37.07	−415.12	452.19	502.11
	pro	−134.01	−134.01	268.02	268.02	−231.29	−231.29	462.58	462.58
	obl	173.70	−347.40	173.70	347.40	279.06	−558.12	279.06	558.12
^{194}Hg	tri1	66.51	−304.41	237.90	320.09	106.10	−494.90	388.80	521.12
	tri2	105.22	−328.24	223.02	335.21	167.71	−531.03	363.32	542.90
	tri3	−4.38	−260.97	265.35	303.91	−57.86	−400.49	458.35	499.21
	pro	−118.50	−118.50	237.00	237.00	−194.90	−194.90	389.80	389.80
	obl	166.21	−332.42	166.21	332.42	271.16	−542.32	271.16	542.32
^{196}Hg	tri1	59.85	−284.96	225.11	300.50	79.55	−448.88	369.33	479.05
	tri2	96.81	−311.28	214.47	318.60	140.55	−492.22	351.67	507.09
	tri3	18.73	−254.27	235.54	283.41	9.84	−399.09	389.25	455.25
	pro	−114.72	−114.72	229.44	229.44	−189.07	−189.07	378.14	378.14
	obl	156.31	−312.62	156.31	312.62	258.08	−516.16	258.08	516.16
^{198}Hg	tri1	55.32	−278.27	222.95	294.62	68.43	−437.65	369.22	470.85
	tri2	89.94	−292.44	202.50	299.57	122.77	−459.51	336.74	475.82
	tri3	21.06	−237.14	216.08	262.52	15.19	−374.68	359.49	424.15
	pro	−100.94	−100.94	201.88	201.88	−166.93	−166.93	333.86	333.86
	obl	154.00	−308.00	154.00	308.00	254.93	−509.86	254.93	509.86
^{200}Hg	tri1	55.85	−257.90	202.05	271.37	70.74	−405.93	335.19	433.69
	tri2	84.99	−265.39	180.40	271.05	114.69	−416.45	301.76	430.23
	tri3	22.12	−232.60	210.48	256.77	19.11	−369.33	350.22	415.87
	pro	−39.56	−39.56	79.12	79.12	−55.06	−55.06	110.12	110.12
	obl	70.02	−140.04	70.02	140.04	113.76	−227.52	113.76	227.52
^{202}Hg	tri1	11.03	−83.20	72.17	90.37	18.49	−120.95	102.46	130.31
	tri2	43.36	−133.07	89.71	135.73	74.89	−219.77	144.88	223.45
	tri3	−10.68	−75.11	85.79	93.51	−8.36	−115.66	124.02	138.63
	pro	−18.66	−18.66	37.32	37.32	−25.59	−25.59	51.18	51.18
	obl	20.83	−41.66	20.83	41.66	29.83	−59.66	29.83	59.66
^{204}Hg	tri1	3.34	−41.98	38.64	46.66	7.37	−62.21	54.84	67.98
	tri2	13.13	−55.20	42.07	57.68	21.19	−82.74	61.55	85.96
	tri3	−7.16	−43.35	50.51	54.66	−7.37	−65.81	73.18	80.59

TABLE II. (*Continued*).

		Proton (fm^2)				Neutron (fm^2)			
		Q_x	Q_y	Q_z	Q_0	Q_x	Q_y	Q_z	Q_0
	pro	−12.33	−12.33	24.66	24.66	−15.52	−15.52	31.04	31.04
	obl	14.34	−28.68	14.34	28.68	16.97	−33.94	16.97	33.94
^{206}Hg	tri1	1.53	−29.53	28.00	33.25	1.39	−36.87	35.48	41.80
	tri2	9.63	−43.47	33.84	45.67	12.09	−55.86	43.77	58.78
	tri3	−6.16	−32.42	38.58	41.45	−8.48	−42.34	50.82	54.45
	pro	−24.40	−24.40	48.80	48.80	−50.61	−50.61	101.22	101.22
	obl	28.82	−57.64	28.82	57.64	58.15	−116.30	58.15	116.30
^{208}Hg	tri1	15.49	−58.87	43.38	61.03	29.79	−118.04	88.25	122.77
	tri2	25.76	−72.77	47.01	73.79	45.97	−135.83	89.86	138.18
	tri3	0.03	−59.00	58.97	68.11	7.15	−118.33	111.18	132.70
	pro	−46.50	−46.50	93.00	93.00	−99.30	−99.30	198.60	198.60
	obl	30.01	−60.02	30.01	60.02	67.57	−135.14	67.57	135.14
^{210}Hg	tri1	6.92	−58.38	51.46	63.80	15.08	−130.03	114.95	142.24
	tri2	20.88	−74.15	53.27	76.47	41.16	−151.41	110.25	156.57
	tri3	−14.86	−61.06	75.92	80.47	−33.03	−130.68	163.71	173.14

III. RESULTS AND DISCUSSION

We use the Skyrme parameter set SKI4 to calculate the ground-state properties of Hg isotopes. For a given nucleus the solution which corresponds to the maximum binding energy is the ground state of the nucleus. The numerical results on binding energies of Hg isotopes are been listed in Table I. The RMF results with NL1 are also listed for comparison. In the table Expt. is the experimental data 23 or the estimated value (denoted as #) as the experimental values are unknown [23]. The spherical (sph), prolate (pro), oblate (obl) and triaxial (tri1, tri2, and tri3) solutions are also listed in the table for comparison. In the meantime we plot the binding energy per nucleon (B/A) in Fig. 1. The binding energies calculated with the SKI4 agree well with experimental data [23] and the relative difference of the binding energy is at most 0.3%. The ground states which correspond to the maximum binding energy are oblate for ^{170}Hg–^{196}Hg, triaxial for ^{198}Hg and ^{200}Hg, spherical for ^{202}Hg–^{206}Hg, and triaxial for ^{208}Hg and ^{210}Hg, respectively. It is well known that there is the shape coexistence in Hg isotopes. Our calculation agrees with this. It is seen from Table I that the energy minima of the oblate and triaxial solutions lie closer than that of the oblate and prolate solutions. These indicate that the structures of Hg isotopes are more complicated than the previous results which show that there is only a shape coexistence between prolate ellipsoid and oblate ellipsoid.

We plot in Fig. 2 the absolute difference of the binding energies between theoretical results and experimental data. It is obvious that the results of SKI4 are better than that of NL1 and the absolute difference is less than 2 MeV except for ^{206}Hg (about 5 MeV). For nuclei far from the stable line, NL1 has a large error (about 14 MeV), but the results of SKI4 are excellent. It proves that the force SKI4 can give reliable results for nuclei not only near the stable line but also far from the stable line because the nucleon-nucleon correlations have been treated carefully and the isospin degrees of freedom have been included in the force SKI4.

The two-neutron separation energy of Hg isotopes is plotted in Fig. 3 where it has been defined as the difference of binding energies $S_{2n}(Z,N)=B(Z,N)-B(Z,N-2)$. The results of SKI4 agree well with the experimental values. Because of the shell effects, there is a dramatic decrease in ^{208}Hg in Fig. 3.

In Fig. 4, we plot the isotope shift $r_c^2(A)-r_c^2(\mathrm{ref})$ for Hg nuclei (^{198}Hg is chosen as a reference nucleus in the Hg chain). The empirical data obtained from atomic laser spectroscopy are also shown by the solid circles [24]. The theoretical values from the deformed Skyrme-Hartree-Fock (DSHF) model and from the spherical Skyrme-Hartree-Fock (SSHF) model are denoted by open circles and open squares in the figure, respectively. It is seen from the figure that the DSHF model with SKI4 is successful in reproducing the isotope shift of Hg nuclei and the SSHF model has an obvious difference from the experimental data except for the spherical nuclei ^{202}Hg–^{206}Hg. It indicates that there exists the deformation in Hg isotopes when the neutron number N is below the reference point. The DSHF model with SKI4 is successful in reproducing both the binding energy and the nuclear charge radius. As the isotope shifts in a chain of isotopes are the variation of proton distributions with neutron number, it is evident that the isotope shift depends on the correlations between protons and neutrons. The force SKI4, which has the generalized spin-orbit term, treats the correlations between protons and neutrons correctly.

The calculated root-mean-square radii of the density distributions of protons, neutrons, matter, and charge (r_p, r_n, r_t, and r_c, respectively) in the DSHF model are plotted in Fig. 5. The rms matter radius has been calculated by defining the total radius as the average of proton and neutron radii in every orbit weighted with occupation probabilities. The charge radius is obtained from the charge density which is obtained from the charge form factor by the inverse Fourier-

TABLE III. The proton and neutron hexadecupole moments Q_{40}, Q_{42}, and Q_{44} and hexadecupole deformations parameters β_4, γ_4 (in degrees), and δ_4 (in degrees) obtained with the SKI4 for three triaxial cases.

		Proton						Neutron					
		Q_{40}	Q_{42}	Q_{44}	β_4	γ_4	δ_4	Q_{40}	Q_{42}	Q_{44}	β_4	γ_4	δ_4
^{170}Hg	tri1	308	−22	−297	0.012	25	66	1051	276	−71	0.010	−1	77
	tri2	278	41	−241	0.012	24	52	687	362	28	0.008	−10	83
	tri3	703	−141	−298	0.012	32	81	1332	104	−129	0.012	10	65
^{172}Hg	tri1	420	−44	−290	0.012	32	59	975	258	−60	0.008	3	85
	tri2	241	32	−229	0.013	27	48	652	364	40	0.007	−6	73
	tri3	497	−140	−296	0.011	39	67	1074	122	−127	0.008	16	78
^{174}Hg	tri1	227	−37	−282	0.012	36	48	711	286	−46	0.006	6	71
	tri2	181	17	−211	0.013	31	46	590	345	68	0.007	3	62
	tri3	277	−71	−280	0.011	44	48	738	237	−108	0.005	9	65
^{176}Hg	tri1	132	53	−226	0.011	36	38	545	435	35	0.005	−13	47
	tri2	147	73	−143	0.012	32	41	549	453	181	0.006	−7	54
	tri3	−18	−40	−275	0.011	58	32	298	286	−97	0.005	−5	19
^{178}Hg	tri1	11	53	−203	0.011	38	33	353	442	84	0.005	−25	36
	tri2	150	148	−61	0.011	28	38	552	595	332	0.005	−26	53
	tri3	−134	298	−260	0.011	58	27	116	298	−67	0.006	−24	9
^{180}Hg	tri1	108	108	−130	0.010	34	35	489	548	230	0.005	−31	46
	tri2	212	214	26	0.010	22	39	659	725	512	0.005	−38	67
	tri3	−87	−27	−237	0.010	53	30	169	300	−24	0.005	−19	14
^{182}Hg	tri1	241	147	−66	0.010	31	40	710	630	365	0.005	−24	59
	tri2	300	261	97	0.010	16	44	813	825	665	0.005	−36	71
	tri3	−33	−51	−220	0.011	63	32	163	178	10	0.007	89	22
^{184}Hg	tri1	201	76	−88	0.011	38	41	631	508	311	0.005	6	45
	tri2	185	152	21	0.011	30	40	606	637	518	0.006	−8	47
	tri3	53	−47	−250	0.011	52	37	304	288	−72	0.007	29	23
^{186}Hg	tri1	119	−16	−151	0.012	48	41	449	330	167	0.009	36	37
	tri2	147	98	−25	0.013	38	40	476	505	389	0.010	21	36
	tri3	42	−93	−267	0.012	58	38	197	189	−117	0.009	62	24
^{188}Hg	tri1	93	−77	−202	0.014	52	41	335	172	25	0.012	52	37
	tri2	26	−22	−134	0.015	45	39	211	243	135	0.014	43	35
	tri3	−10	−145	−294	0.013	64	37	−3	68	−191	0.012	83	26
^{190}Hg	tri1	20	−185	−277	0.016	57	42	176	−63	−156	0.016	60	40
	tri2	−10	−101	−211	0.018	49	40	87	24	−84	0.018	49	38
	tri3	−164	−230	−321	0.015	73	37	−412	126	−255	0.016	−78	29
^{192}Hg	tri1	−27	−282	−333	0.018	59	43	80	−290	−300	0.019	62	43
	tri2	−110	−248	−349	0.020	52	41	−82	−279	−385	0.023	52	40
	tri3	−309	−279	−286	0.016	87	36	−853	−304	−214	0.020	−61	33
^{194}Hg	tri1	−128	−344	371	0.019	62	43	−118	−451	−394	0.021	66	42
	tri2	−159	−309	−385	0.021	55	41	−191	451	−511	0.024	55	41
	tri3	−714	−375	−239	0.019	−72	35	−1826	−607	−122	0.026	−47	39

TABLE III. (*Continued.*)

		Proton						Neutron					
		Q_{40}	Q_{42}	Q_{44}	β_4	γ_4	δ_4	Q_{40}	Q_{42}	Q_{44}	β_4	γ_4	δ_4
	tri1	−568	−503	−276	0.020	85	40	−1349	−1049	−122	0.025	−77	45
^{196}Hg	tri2	−465	−435	−313	0.020	70	39	−1129	−943	−278	0.025	86	41
	tri3	−675	−558	−160	0.019	−77	44	−1589	−1105	130	0.025	−60	51
	tri1	−809	−546	−201	0.020	−83	39	−2021	−1266	26	0.029	−65	47
^{198}Hg	tri2	−771	−558	−277	0.022	86	38	−1916	−1320	−154	0.029	−76	44
	tri3	−1099	−685	−114	0.022	−66	45	−2481	−1404	241	0.030	−53	52
	tri1	−1230	−603	−165	0.023	−68	38	−2856	−1439	118	0.032	−56	47
^{200}Hg	tri2	−1089	−687	−252	0.023	−82	39	−2598	−1612	−59	0.032	−66	46
	tri3	−1421	−618	−57	0.023	−54	42	−3182	−1387	362	0.033	−45	50
	tri1	−265	−141	−78	0.004	−71	37	−470	−241	−212	0.005	−81	32
^{202}Hg	tri2	−581	−472	−458	0.014	77	38	−1247	−1028	−1109	0.020	73	37
	tri3	−298	−86	−20	0.004	−38	39	−528	−153	−96	0.005	−45	33
	tri1	−84	−36	−34	0.001	−73	30	−213	−61	−92	0.002	−69	22
^{204}Hg	tri2	−78	−42	−46	0.002	86	30	−199	−76	−111	0.002	89	24
	tri3	−89	−30	−22	0.001	−52	32	−235	−57	−73	0.002	−49	25
	tri1	−10	10	−14	0.001	−47	22	−98	13	−74	0.001	−38	8
^{206}Hg	tri2	−13	12	−11	0.001	−51	15	−101	18	−66	0.001	−57	6
	tri3	−1	9	−16	0.001	−32	29	−83	12	−75	0.001	−29	9
	tri1	343	271	141	0.005	−78	45	1032	897	435	0.011	−80	48
^{208}Hg	tri2	275	256	181	0.005	−89	45	814	854	580	0.010	−83	48
	tri3	423	271	93	0.006	−65	47	1371	915	260	0.012	−64	49
	tri1	235	−7	−197	0.004	5	85	776	30	−661	0.008	1	85
^{210}Hg	tri2	69	−25	−204	0.003	12	58	213	17	−628	0.006	3	58
	tri3	532	−27	−126	0.005	7	61	1886	−65	−438	0.012	5	60

Bessel transform. We can see from Fig. 5 that the radii increase smoothly with neutron number. The RMF-NL1 results [6] show that the various radii have a dramatic increase at $A=180$ and oscillations below $A=188$. The authors of Refs. [6, 8] notice it but they do not give a satisfying explanation [6,8]. The previous nonrelativistic HF+BCS calculations seem to fail in reproducing the experimental trend [2]. We analyze why the radii have a smooth increase with neutron number in our calculation. There are three causes: (i) For ^{170}Hg–^{200}Hg, the binding energies in oblate solutions (or triaxial solutions) are greater than those in prolate solutions (about 1–4 MeV) and so there is no prolate ellipsoid for the ground state of these nuclei. The binding energies in triaxial solutions are very close to oblate shape and γ_2 in the triaxial cases (see Table I) is close to 60°. Therefore there is no dramatic change of nuclear shape in our results. This is different from previous results which show that there is a shape transition from oblate to prolate or from prolate to oblate [6]. In our calculation, the SKI4 results show only a smooth shape transition from oblate to triaxial at first, then to spherical, and finally to triaxial shape. Because it is only a smooth shape transition, the radii have a similar smooth variation. (ii) There is no superdeformed ground state in our results and thus this avoids a dramatic change of radii. The oblate and triaxial configurations are almost degenerate for ^{170}Hg–^{200}Hg in our calculation. This is different from other papers, which show that there are only axial deformations of prolate and oblate ellipsoids. (iii) SKI4 can reproduce the experimental data of the ground-state properties for nuclei far from the stable line due to the modification of the spin-orbit term in effective forces.

The deformations of nuclei play a crucial role in the ground state of nuclei. In Table II, we show the numerical results of the quadrupole moments Q_x, Q_y, Q_z, and Q_0 which are defined in Eqs. (5)–(9). For the prolate case, $Q_x=Q_y=-Q_z/2$ and $Q_0=Q_z$. For the oblate case, $Q_x=Q_z=-Q_y/2$ and $Q_0=|Q_y|$. For triaxial cases, only $Q_x+Q_y+Q_z=0$. We can see from Table II that there are smaller quadrupole moments in prolate configurations than those in oblate configurations. The quadrupole moments in triaxial configurations are close to those in oblate configurations. ^{202}Hg–^{206}Hg are spherical nuclei because they have very small quadrupole moments.

The quadrupole deformation parameters β_2 and γ_2 are

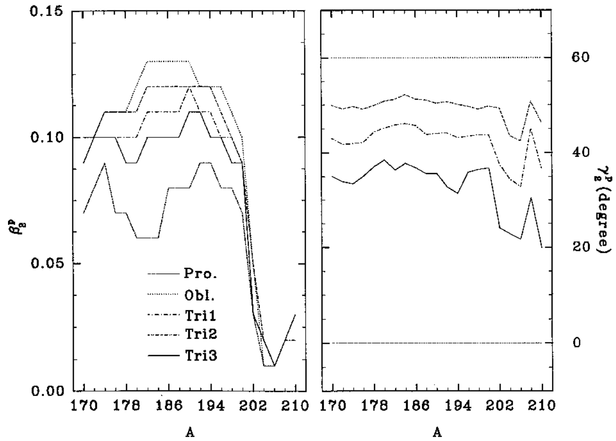

FIG. 6. The quadrupole deformation parameters β_2 (left plot) and γ_2 (right plot) in the ground state of Hg isotopes as a function of the mass number.

also listed in Table I. We also plot the β_2 and γ_2 of Hg isotopes as a function of the mass number in Fig. 6. In the prolate case, $\gamma = 0°$; in the oblate case, $\gamma_2 = 60°$; and in the triaxial cases, $0° < \gamma_2 < 60°$. We compare our results with the RMF-NL1 results and find that NL1 reproduces a large prolate deformation β_2 for ^{176}Hg–^{192}Hg. The SKI4 results for β_2 agree well with the experimental values. The triaxial solutions of γ_2 are close to 60° and this indicates that the shape transition will be a smooth change. There are no superdeformed solutions in the ground state of these nuclei but there are triaxial solutions for ^{198}Hg, ^{200}Hg, ^{208}Hg, and ^{210}Hg. For ^{198}Hg and ^{200}Hg, γ_2^p is 49.13° and 49.72°, respectively. These values are close to oblate shape ($\gamma_2^p = 60°$ for the oblate case). For ^{208}Hg and ^{210}Hg, $\beta_2^p = 0.03$. It is small and close to spherical shape ($\beta_2^p = 0$ in the spherical case). It is concluded from Table I that there exists a shape coexistence in the ground state of Hg isotopes. For ^{170}Hg–^{200}Hg, there is the shape coexistence between the oblate ellipsoid and triaxial shape but the binding energies of oblate solutions are slightly larger than those of the triaxial solutions for ^{170}Hg–^{196}Hg and the binding energies of triaxial solutions are slightly larger than those of the oblate solutions for ^{198}Hg and ^{200}Hg. ^{202}Hg–^{206}Hg are approximately spherical. For ^{208}Hg and ^{210}Hg, there is various shape coexistences but the binding energies of the triaxial solutions are slightly larger than those of other solutions. There exists a shape transition in the ground-state of Hg isotopes: from oblate to triaxial shape in ^{198}Hg, from triaxial to spherical shape in ^{202}Hg, and from spherical to triaxial shape in ^{208}Hg.

Finally, we list the hexadecupole moments Q_{40}, Q_{42}, and Q_{44} and the hexadecupole deformation parameters $\gamma_4^{n,p}$, $\beta_4^{n,p}$, and $\delta_4^{n,p}$ in Table III for the triaxial cases. These quantities may be useful for fusion cross sections. For the cases tri1 and tri2, Q_{40} has a sign change from positive to negative near ^{198}Hg. Because of the small β_4 ($\beta_4 < 0.03$ except for ^{198}Hg and ^{200}Hg), we think that the hexadecupole deformations are not important for Hg isotopes.

IV. CONCLUSION

In this paper, we use the deformed-Skyrme-Hartree-Fock model with new Skyrme parameter set SKI4 to calculate the ground-state properties of Hg isotopes. The numerical results agree well with the experimental data. We summarize our main results as follows. (i) The new Skyrme parameter set SKI4, which has a generalized spin-orbit term, is successful in reproducing the binding energies, isotope shifts, and radii both for nuclei near the stable line and for exotic nuclei far from the stable line. (ii) The deformation parameter obtained by SKI4 (β_2) agrees well with the experimental values. There is the shape coexistence for the ground state of Hg isotopes: ^{170}Hg–^{200}Hg are oblate shape or have a shape coexistence between oblate and triaxial shape. ^{202}Hg–^{206}Hg are spherical shape or have a shape coexistence among spherical, triaxial, and oblate shapes. ^{208}Hg and ^{210}Hg are triaxial shape or of various shape coexistences. There is no superdeformed ground state for Hg isotopes in the DSHF calculation with SKI4. (iii) The calculated radii from the force SKI4 show a smooth increase with neutron number and they agree well with the experimental trend. This can be understood because the shape transition of Hg isotopes is smooth. (iv) Because our large-scale calculations have almost exhausted all possible configurations of deformations, the conclusions are very reliable.

ACKNOWLEDGMENTS

Z.R. would like to thank Prof. Faessler for discussions. This work was supported by the Alexander von Humboldt Foundation of Germany and by the National Natural Science Foundation of China.

[1] J. H. Hamilton, P. G. Hansen, and E. F. Zganjar, Rep. Prog. Phys. **48**, 631 (1985).
[2] J. Bohn, G. Huber, H. J. Kluge, L. Kugler, and E. Otten, Phys. Lett. **38B**, 308 (1972).
[3] E. Otten, in *Treatise on Heavy-Ion Science*, edited by D. A. Bromley (Plenum, New York, 1989), Vol. 8.
[4] I. Tanihata *et al.*, Phys. Rev. Lett. **55**, 2676 (1985).
[5] R. Bengtsson, T. Bengtsson, J. Dudek, G. Leander, W. Nazarewicz, and J. Y. Zhang, Phys. Lett. B **183**, 1 (1987).
[6] S. K. Patra, S. Yoshida, and N. Takigawa, Phys. Rev. C **50**, 1924 (1994).
[7] S. Yoshida, S. K. Patra, N. Takigawa, and C. R. Praharaj, Phys. Rev. C **50**, 1398 (1994).
[8] N. Takigawa, S. Yoshida, K. Hagina, and S. K. Patra, Phys. Rev. C **53**, 1038 (1995).
[9] K. Heyde, C. De Coster, P. Van Duppen, M. Huyse, J. L. Wood, and W. Nazarewicz, Phys. Rev. C **53**, 1035 (1995).
[10] P. Bonche, S. J. Krieger, P. Quentin, M. S. Weiss, J. Meyer, M. Meyer, N. Redon, H. Flocard, and P. H. Heenen, Nucl. Phys. **A500**, 308 (1989).

[11] P. Bonche, J. Dobaczewski, H. Flocard, P. H. Heenen, S. J. Krieger, J. Meyer, and M. S. Weiss, Nucl. Phys. **A519**, 509 (1990).

[12] P. Bonche, S. J. Krieger, M. S. Weiss, J. Dobaczewski, H. Flocard, and P. H. Heenen, Phys. Rev. Lett. **66**, 876 (1991).

[13] P. Bonche, H. Flocard, P. H. Heenen, S. J. Krieger, and M. S. Weiss, Nucl. Phys. **A443**, 39 (1985).

[14] Naoki Tajima, Satoshi Takahara, and Naoki Onishi, Nucl. Phys. **A603**, 23 (1996).

[15] D. Hirata, K. Sumiyoshi, B. V. Carlson, H. Toki, and I. Tanihata, Nucl. Phys. **A609**, 131 (1996).

[16] J. L. Wood, K. Heyde, W. Nazarewicz, M. Huyse, and P. Van Duppen, Phys. Rep. **215**, 103 (1992).

[17] N. Tajima, P. Bonche, H. Flocard, P. H. Heenen, and M. S. Weiss, Nucl. Phys. **A551**, 434 (1993).

[18] P. G. Reinhard and H. Flocard, Nucl. Phys. **A584**, 467 (1995).

[19] Yao-song Shen and Zhongzhou Ren, Z. Phys. A **355**, 247 (1996); **356**, 133 (1996).

[20] Yao-song Shen and Zhongzhou Ren, Phys. Rev. C **54**, 1158 (1996).

[21] Yao-song Shen, XiaoFen Zhu, and Zhongzhou Ren, Chin. Phys. Lett. **15**, 404 (1998).

[22] H. Sagawa and H. Toki, J. Phys. G **13**, 453 (1987).

[23] G. Audi and A. H. Wapstra, Nucl. Phys. **A565**, 1 (1993).

[24] H. de Vries, C. W. de Jager, and C. de Vries, At. Data Nucl. Data Tables **462**, 455 (1987).